A mechanical energy budget for the North Sea

Knut Barthel [a], Herman G. Gade[a] and Cathrine K. Sandal[b]

[a] Geophysical Institute, University of Bergen, Allégaten 70, Bergen N-5007, Norway
[b] Oceanography Department, 0102 OSB, West Call Street, Florida State University, Tallahassee, FL 32306-4320, USA

Received 19 February 2003; revised 8 September 2003; accepted 16 October 2003.

Abstract

A three-dimensional baroclinic numerical model is used to quantify the components of the mechanical energy budget for a semi-enclosed sea, the North Sea. As anticipated, tidal energy is the largest supplier of mechanical energy to the North Sea. Although the energy supply due to winds is responsible for the seasonal variations occurring in the budget, it is one order of magnitude smaller than that due to tides. Most of the input tidal energy is dissipated, specifically in the shallow southern region. Estimates of dissipation and energy flux due to tidal activity are compared to earlier calculations in an attempt to partially validate the results.

Author Keywords: Energy; Budget; Mechanical; Numerical; Tidal; Wind; North Sea

1. Introduction

Practically everywhere in the ocean there are mechanical energy fluxes and conversions. The qualitative processes controlling them are documented; however, considering the quantitative relationships much is unknown. Although some specific cases associated with the energetics of filaments, jets, eddies ([Røed and Shi (1999)]), warm core rings ([Kunze et al (1995)]), El Niño, La Niña ([Goddard and Philander (2000)]), frontal zones ([Erasmi et al (1998)]), outflows ([Baringer and Price (1997)]) and tides ([Jeffreys (1920)]; [Heiskanen (1921)]; [Jeffreys (1952)]; [Miller (1966)]; [Flather (1976)]; [Provost and Lyard (1997)]; [Davies and Kwong (2000)]) are fairly well quantified; an attempt at balancing a mechanical energy budget has yet to be undertaken.

The reason for this apparent lack of knowledge is the fact that governing elements needed for the determination of quantitative relationships have not been possible to observe or quantify with adequate spatial resolution. Foremost, this concerns the fixation of the free surface; however, the absolute velocity field has also proven difficult to determine. As a first effort to this end, a numerical model is used to quantify these components, in an attempt to balance a mechanical energy budget for the North Sea. Results are compared to estimates of dissipation acquired for the North Sea by several authors, in an effort of validation.

A general theory of the mechanical energy budget is presented in Chapter 2. Details concerning the numerical simulations are located in Chapter 3. Results are presented in Chapter 4, and a discussion and comparison with earlier work are given in Chapter 5, with a subsequent conclusion in Chapter 6.

2. The mechanical energy equation for a fixed region

If internal sources and sinks of thermal (internal) energy are insignificant and likewise if geothermal heating of the bottom water is negligible, the general energy equation, containing both thermal and mechanical terms, may be separated into two nearly independent equations, each referring to either purely mechanical or thermal energy forms. In the ocean solar radiation does penetrate into the water column and produces internal heating. However, absorption is usually so great that an overwhelming part of the incoming energy is converted to heat within the upper few meters. As a conservative estimate, less than 10% of the energy reaches a depth of 10 m. Although the North Sea is generally quite shallow, heating of the interior resulting from solar radiation is greatly dominated by vertical eddy exchange with the surface water where absorption is efficient. We have therefore felt justified to separate the thermal and mechanical terms of the energy budget, and dealt with thermal variation of the density as a consequence of vertical eddy diffusion, apart from advection.

We assume a hydrostatic and incompressible fluid. Let the reference level for the potential energy be located at the geopotential level surface z=0. Then the water mass of a fixed region A has a potential energy P given by the volume integral

$$P(t) = \int_A \int \int_{-H}^{\zeta} \rho g z \, dz \, dy \, dx. \tag{2.1}$$

The depth of the sea floor is given by H. The density of seawater, ρ, and the sea surface elevation, ζ, both vary spatially and temporally yielding a time-varying potential energy $P(t)$. The kinetic energy K of the same water mass is given by

$$K(t) = \int_A \int \int_{-H}^{\zeta} \rho \frac{1}{2}(u^2 + v^2) \, dz \, dy \, dx. \tag{2.2}$$

By multiplication of the momentum equation by the current vector (u,v,w), and the continuity equation by the kinetic energy per unit mass, and in a second step by the gravitational potential, $-gz$, and then integrating, we arrive at the mechanical energy equation for a fixed region

$$\frac{d(K+P)}{dt} + \int_S \int \left(\rho \frac{u^2 + v^2}{2} + \rho g z + p \right) \vec{v} \cdot \vec{n} \, dS = W + T - \Gamma. \tag{2.3}$$

In Eq. (2.3), we have used Gauss' divergence theorem. dS is a surface element, and the surface integral is taken over all open boundaries of the region. In this case study, the ensemble of open boundaries S is comprised by the horizontal surface A, and the vertical boundary surfaces S1, S2, and S3 that define A,

see Fig. 1. Γ is energy dissipation, *W* is the wind forcing, and *T* is the tidal forcing. This equation states that kinetic and potential energy of a fixed region change in time due to the transport of kinetic and static energy through open boundaries, sources (wind and tides) and sinks (dissipation).

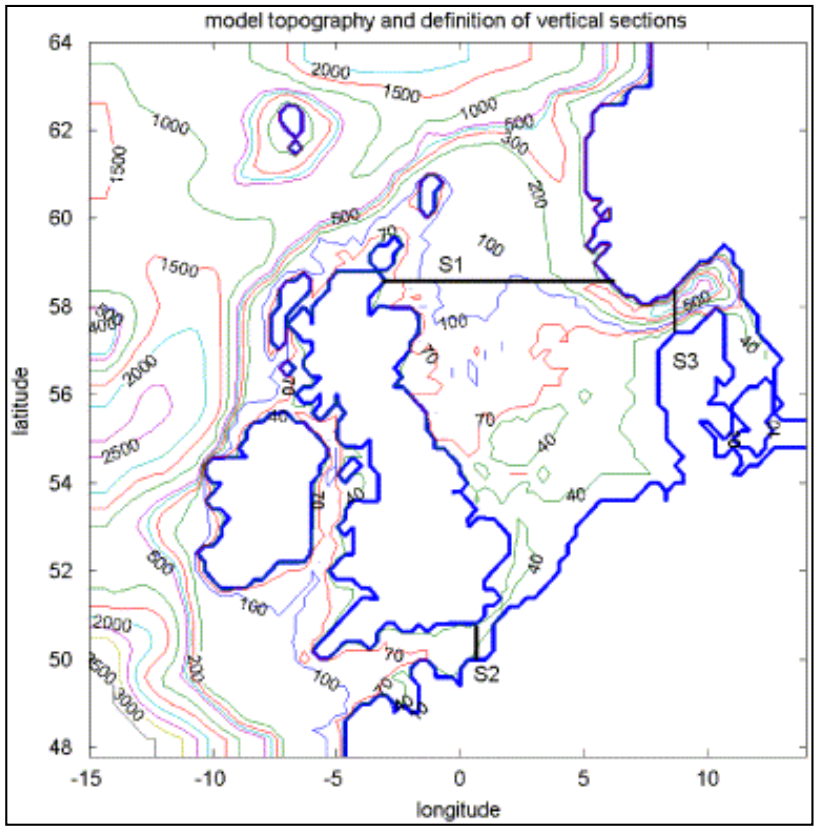

Fig. 1. Model topography, the contour interval is 30 m for the first 100 m, then every 100 m up to 500 m, and thereafter every 500 m. Section 1 is located at latitude 58°36′N running from Scotland to Norway, Section 2 is located at longitude 0°40′E crossing the English Channel, and Section 3 is located at longitude 8°40′E cutting across Skagerrak.

The direct tide generating force is neglected in this model. The co-oscillating tide is included by prescribed values of tidal amplitude and phase along the open model boundaries, i.e. along the longitude 15°W, and the latitudes 64°N and 47°48′N (Fig. 1). (Note the difference between model boundaries and the boundaries of the energy budget region A.) *T* in Eq. (2.3) is the rate of energy supplied through tides, and is evaluated by an indirect approach. The transports of static or kinetic energy across the three vertical Sections S1, S2, and S3 are calculated at each time step, and in addition from the respective daily means of the current velocity. The difference in these two calculations may be attributed to the energy supplied through tides. Let $s = \bar{s} + s'$ and $v = \bar{v} + v'$ denote energy and current, respectively, where the bar denotes a daily average. The daily average of the product is then

$$\overline{sv} = \overline{(\bar{s} + s')(\bar{v} + v')} = \overline{\bar{s}\bar{v}} + \overline{s'v'}. \qquad (2.4)$$

Here the left-hand side is derived from the time step calculations, while the first term on the right-hand side is calculated from the daily mean values. It is this term that gives the transport of energy by the residual current (the integral term on the left-hand side of Eq. (2.3)), such that the second term on the right-hand side gives the tidal energy flux, $-T$.

Our study area is the North Sea, which is semi-enclosed, with open boundaries being the air–sea interface, and three vertical sections defined in Fig. 1. The area inside these three vertical sections is our fixed region A, for which the mechanical energy budget given by Eq. (2.3) is quantified. A numerical ocean circulation model is applied to the entire region depicted in Fig. 1, giving the necessary parameters to calculate each component of the budget. See Appendix A for the formulations of the component calculations.

The processes incorporated in the energy household of the North Sea may be studied in an energy flow diagram (Fig. 2). Here, the North Sea system is represented by the dashed box.

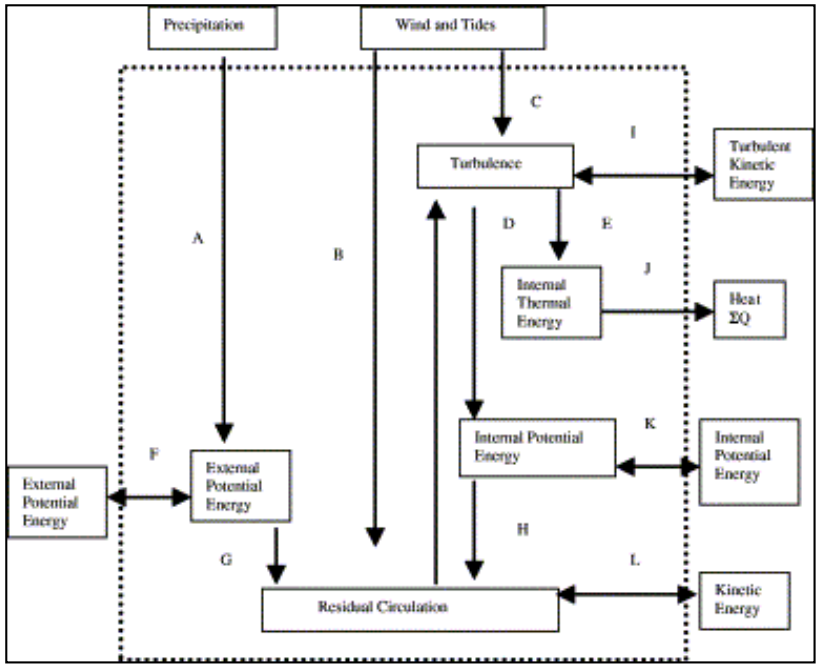

Fig. 2. Simplified flow diagram of mechanical and thermal energy in a shelf sea; (A) supply of potential energy by net precipitation; (B) generated wind drift and rectified tidal circulation; (C) energy conversion to turbulence; (D) conversion of turbulence to internal potential energy; (E) conversion of turbulence to heat; (F) advection of external potential energy to/from system; (G) conversion of external potential energy to residual circulation; (H) conversion of internal potential energy to residual circulation; (I) net export/import of turbulent kinetic energy in the system; (J) loss of generated internal thermal energy (heat) from the system;

(K) net export/import of internal potential energy in the system; and (L) net export/import of kinetic energy by residual circulation.

Energy transfer takes place through the boundaries by various mechanisms. Three sources are depicted outside the box. The first of these, designated External Potential Energy, is supplied either by (1) fresh water at the surface through rivers, (2) the entering currents of the region or (3) a combination of both. Part of this energy strengthens the residual circulation of the system, and some is re-exported as non-available potential energy. The remaining two boxes are Precipitation, and Wind and Tides. Concerning the latter of these two, the corresponding flow of energy can in principle be determined from knowledge of the wind field and from the behaviour of the tides in the region.

In this diagram there are two sinks for this energy flux. One is the maintenance of turbulence and the other is the contribution to residual circulation. The former is mostly an intermediate stage to further transformation; however, it has also direct outside communication; turbulent kinetic energy. Three other communication lines connect to the turbulence box. The first is a source line from residual circulation, which for practical purposes is usually omitted and the associated energy transfer dealt with as if coming directly from Wind and Tides. The two other lines indicate transformation to internal potential energy (work against gravity) and internal thermal energy. Although the latter undoubtedly is a two-way process, the net transfer of heat is always a positive exit flux and therefore indicated by a one-way arrow.

Some of the resulting internal potential energy of the system is exported as non-available. The rest is converted to kinetic form as a contribution to the residual circulation of the system.

3. Numerical simulations

Temporal and spatial variation of the density is needed when balancing a mechanical energy budget; which, in effect, means that a baroclinic model must be used. For this study HAMburg Shelf Ocean Model (HAMSOM), a three-dimensional semi-implicit baroclinic circulation model was chosen. Developed by [Backhaus (1985)] to model shelf seas, it has been extensively applied, in particular, to the North Sea region ([Backhaus and Hainbucher (1987)]; [Hainbucher et al (1987)]; [Pohlmann (1996a), Pohlmann (1996b), Pohlmann (1996c) and Pohlmann (1996d)]) and these works show that this model reproduces the hydrodynamic conditions in the North Sea very well. With a prognostic treatment of salinity and temperature, the model is able to discern interannual and monthly variations. Compared to other commonly used explicit shelf sea models, there are several advantages to HAMSOM. Firstly, it is approximately a factor 5 faster; however, most importantly it is not limited by stability considerations for the free surface when simulating ocean/shelf dynamics, which include deep ocean regions. A brief overview of principal assumptions and input data used is given below; however, for details on the numerical formulation of HAMSOM see [Backhaus (1985)].

Incompressibility and hydrostatic equilibrium is assumed, incorporating the Boussinesq approximation. The governing equations are the non-linear equations of motion, the equation of continuity, the transport equation for temperature and salinity, and the equation of state for seawater. At the sea surface, kinematic boundary conditions are applied to give the surface displacement. Prescribed wind stress input fields give the momentum transport. The atmospheric pressure is neglected. Sensible heat fluxes are computed from the temperature of the upper layer and prescribed input fields of wind speed and surface air temperature. Atmospheric data are given as daily values, acquired from ECMWF reanalysed data for the arbitrarily chosen year 1983. The other surface fluxes are derived internally in the model code, assuming constant values of humidity, cloud cover, and precipitation. For the sea bottom quadratic stress terms are applied, and at closed lateral boundaries a no-flux and semi-slip condition is assumed for momentum. The normal derivatives of the mass flux are assumed to vanish at open boundaries. Inflow of Baltic water and river runoff (taken to be the rivers Rhine, Meuse, and Elbe) are introduced as climatologically monthly means. Also, salinity and temperature are specified for the Baltic inflow. Tidal amplitude and phase are prescribed along open boundaries, neglecting any explicit representation of tidal acceleration in the equations of motion. Although tidal activity in the North Sea is both important and known with sufficient accuracy, only the dominant M_2 component is chosen to represent tidal dynamics. [Davies et al (2001)] have found that the current profiles and mixing are influenced by the inclusion of other tidal components. The restriction to only one tidal constituent is a shortcoming of these calculations, but we estimate the discrepancy to be small (about 10% of the tidal effect) and hence not affecting the energy budget calculations to any large degree. Further, a radiation condition to prevent noise of surface displacement fluctuations was applied (Orlanski's absorbing boundary condition). A second-order closure scheme (Kochergin–Pohlmann scheme) is used to compute the vertical

eddy viscosity, see [Pohlmann (1996c)].

The current profile and distribution of mass are approximated by a stepwise vertical integration of properties (impulse form) in 12 model layers of increasing thickness. The thicknesses are from top to bottom: 10, 10, 10, 30, 40, 50, 50, 50, 100, 250, 400, and 2500 m. This type of model, also called a "grid-box" model, allows vertically integrated quantities to be defined within one grid-box. Boxes next to the bottom may have different sizes due to the topography. To avoid unevenness in the bottom friction caused by the step-like structure of the topography, an isotropic friction factor for the bottom stress is computed by integrating the information from the lower near-bottom model layers over a range of 500 m. For the North Sea, this means that the bottom friction is computed applying a depth-mean current velocity.

Fig. 1 shows the model area, which covers a part of the North-western European Shelf, from 15°W to 14°E, and from 47.8°N to 64°N, which embeds the North Sea. The longitudinal and latitudinal resolution is 20′ and 12′, respectively. Thus the longitudinal grid distance varies from 24.9 km in the south to 16.3 km in the north, while the latitudinal grid distance is 22.2 km. The time step is 621 s (which gives an integer number of time steps during the tidal period). The degree of implicitness is 0.65 (0.5 is the neutral Crank–Nicholson scheme). This value and the length of the time step assure numerical damping and dispersion errors to be limited.

Climatologically, monthly mean values of temperature and salinity distributions in the horizontal and the vertical, calculated from observational data covering the period 1968–1985 ([Damm (1989)]), provide input for the initial state of the model. The spatial distribution of density is computed from the temperature and salinity data using the equation of state for seawater. The model is spun up for 1 month, and then run for the full year 1983. Some results of this run are shown below.

Fig. 3 shows the modelled seasonal variation of the mean sea surface displacement. During winter and spring there is a rather small gradient, while during summer and fall this gradient is increased substantially from north to south in the North Sea.

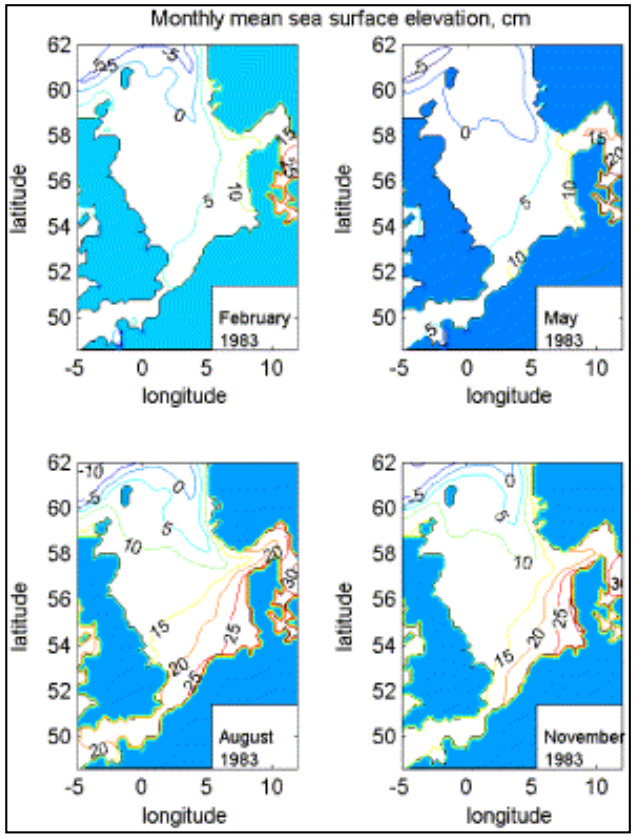

Fig. 3. Modelled monthly mean sea surface elevation for a month in each season.

Fig. 4 displays the modelled monthly mean surface current for August. Clearly, the model captures the prominent current systems of the area, the Norwegian Coastal current, the Dooley Current, and the North Atlantic Drift.

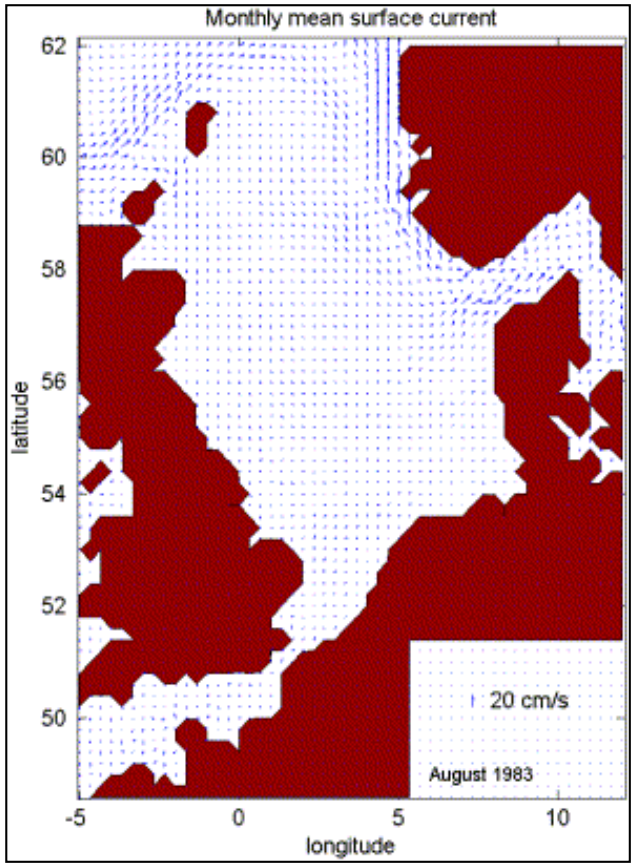

Fig. 4. Modelled monthly mean surface current for August.

4. A mechanical energy budget

Annual and seasonal values for the mechanical energy budget components are given in Table 1. The mechanical energy budget for the North Sea as given by this model shows that tidal static energy input is mainly balanced by dissipation. The input rate of wind energy is one order of magnitude less than the input rate of tidal static energy. Moreover, the transports of static energy with the residual current into and out from the North Sea is one–two order of magnitudes less than the wind input. Table 1 shows that the components of the budget cover five orders of magnitude, where the kinetic energy terms play a minor role.

Table 1. Components of the mechanical energy budget for the North Sea

Component	Annual	January–March	April–June	July–September	October–December
Kinetic energy change	-2.3×10^6	-8.6×10^6	-5.7×10^5	2.4×10^6	-2.3×10^6
Potential energy change	2.2×10^7	-4.4×10^8	7.6×10^8	7.8×10^8	-1.0×10^9
Flux of residual kinetic energy					
S1	2.1×10^6	1.2×10^6	-2.0×10^5	4.8×10^6	2.5×10^6
S2	-7.5×10^5	-5.2×10^5	-2.4×10^5	-1.4×10^5	-2.1×10^6
S3	2.3×10^6	3.2×10^6	-2.7×10^6	3.0×10^6	5.8×10^6
Flux of residual static energy					
S1	8.7×10^7	1.1×10^8	5.8×10^7	-2.7×10^7	2.1×10^8
S2	-1.5×10^8	-9.9×10^7	-6.1×10^7	-2.0×10^8	-2.5×10^8
S3	7.5×10^6	-1.2×10^8	-6.2×10^7	1.5×10^8	5.8×10^7
Flux through the free surface	1.5×10^6	-4.5×10^6	-2.6×10^6	6.0×10^6	7.0×10^6
Rate of wind energy	2.3×10^9	3.0×10^9	1.1×10^9	9.8×10^8	4.0×10^9
Flux rate of tidal kinetic energy					
S1	2.1×10^7	2.5×10^7	1.0×10^7	2.6×10^7	2.4×10^7
S2	3.4×10^7	3.6×10^7	2.4×10^7	3.1×10^7	4.6×10^7
S3	-3.1×10^5	-3.9×10^5	9.8×10^3	-1.9×10^5	-6.7×10^5
Flux rate of tidal static energy					
S1	2.9×10^{10}	2.9×10^{10}	2.9×10^{10}	2.9×10^{10}	2.9×10^{10}
S2	1.8×10^{10}	1.8×10^{10}	1.8×10^{10}	1.8×10^{10}	1.8×10^{10}
S3	1.6×10^8	1.1×10^8	1.4×10^8	2.7×10^8	1.2×10^8
Rate of energy dissipation	4.8×10^{10}	4.9×10^{10}	4.6×10^{10}	4.6×10^{10}	5.0×10^{10}

Units are W.

In Fig. 5, the monthly mean budget terms are grouped according to their order of magnitude. The rate of tidal static energy through Sections S1 and S2 are almost constant, while the rate of energy dissipation varies weakly (Panel e). This variation in dissipation is due to the varying rate of wind energy (Panel d(*)). The potential energy change (Panel d(+)) is positive from March to September, reflecting the build up of the sea surface displacement gradient seen in Fig. 3. Most of the fluctuations in the fluxes of kinetic energy (Panel a) and static energy (Panel c) is found in the Skagerrak section (o). Kinetic energy varies not as systematically as the potential energy (Panel b(+)).

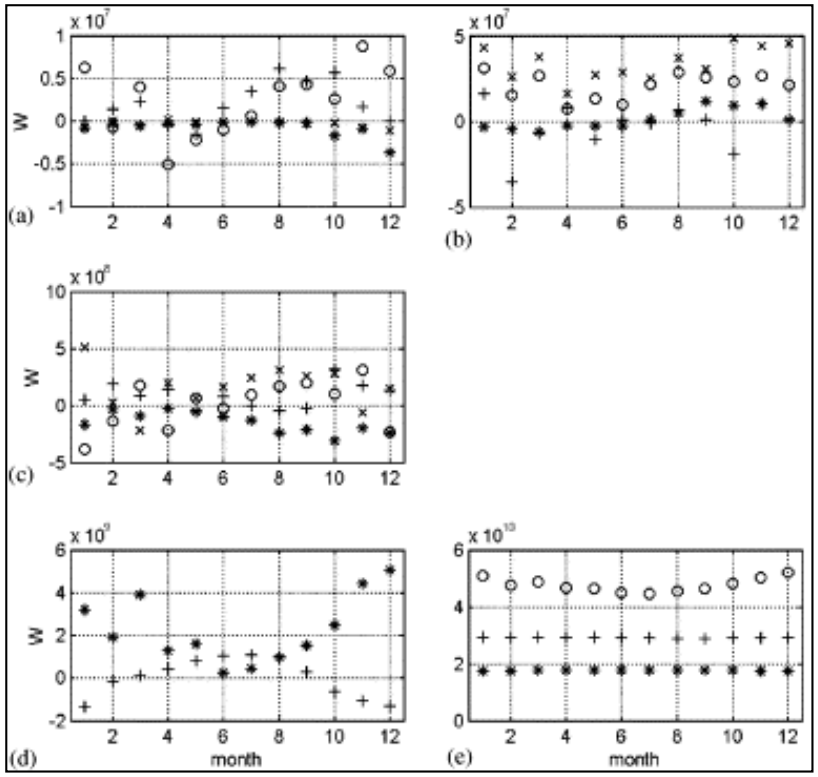

Fig. 5. Monthly mean values of the energy budget terms (in W). Panel (a): Flux of kinetic energy through Section 1 (+), Section 2 (*), Section 3 (o), and rate of tidal kinetic energy through Section 3 (x). Panel (b): Kinetic energy change (+), flux of static energy through the free surface (*), and rate of tidal kinetic energy through Section 1 (o) and Section 2 (x). Panel (c): Flux of static energy through Section 1 (+), Section 2 (*), Section 3 (o), and rate of tidal static energy through Section 3 (x). Panel (d): Potential energy change (+) and rate of wind energy (*). Panel (e): Rate of tidal static energy through Section 1 (+) and Section 2 (*), and rate of energy dissipation (o).

The large seasonal variation of tidal kinetic energy input through all three cross Sections S1–S3 (see row numbers 11–13 in Table 1) reflects covariance of tidal kinetic energy and wind-driven currents through these sections. A similar covariance between tidal static energy and wind-driven currents is only seen at S3 (row number 16), not for S1 and S2 (row numbers 14 and 15).

The dissipation given in Table 1 and in (Panel e) of Fig. 5 contains both physical and numerical damping. The numerical effects can only be determined by balancing the budget, apart from the artificial Coriolis energy, which stems from the model's impulse form and the use of an Arakawa-C grid.

There is an energy sink/source connected to the Coriolis force when the sea floor is sloping, due to the way the *v*-components are interpolated to the *u*-points, and vice versa. (See [Espelid et al (2000)], where it is shown that by four-point averaging the transport divided by the square root of the depth gives an energy conserving treatment of the Coriolis force.) This energy can be calculated explicitly, and the last row in Table 2 gives its contribution to the budget region. The annual mean is -1.7×10^9 W, approximately 3.5% of the total dissipation, and varies only slightly throughout the year.

Table 2. The physical dissipation as determined by Eq. (A.9), the numerical dissipation connected to damping inherent in the model and determined by balancing the budget, and the artificial Coriolis energy

Item	Annual	January–March	April–June	July–September	October–December
Physical dissipation	4.2×10^{10}	4.1×10^{10}	4.2×10^{10}	4.2×10^{10}	4.1×10^{10}
Numerical dissipation	6.2×10^{9}	7.9×10^{9}	3.8×10^{9}	3.6×10^{9}	9.4×10^{9}
Coriolis energy	-1.7×10^{9}	-1.6×10^{9}	-1.6×10^{9}	-1.8×10^{9}	-1.7×10^{9}

Units are W.

An example of the horizontal distribution of this artificial source in the model is shown in Fig. 6 as the monthly mean for December. The most extreme values, –2.38 and 4.58 W m^{-2}, are both found at Pentland Firth, just outside our budget region. For December the integrated value for the budget region is equal to -1.67×10^9 W.

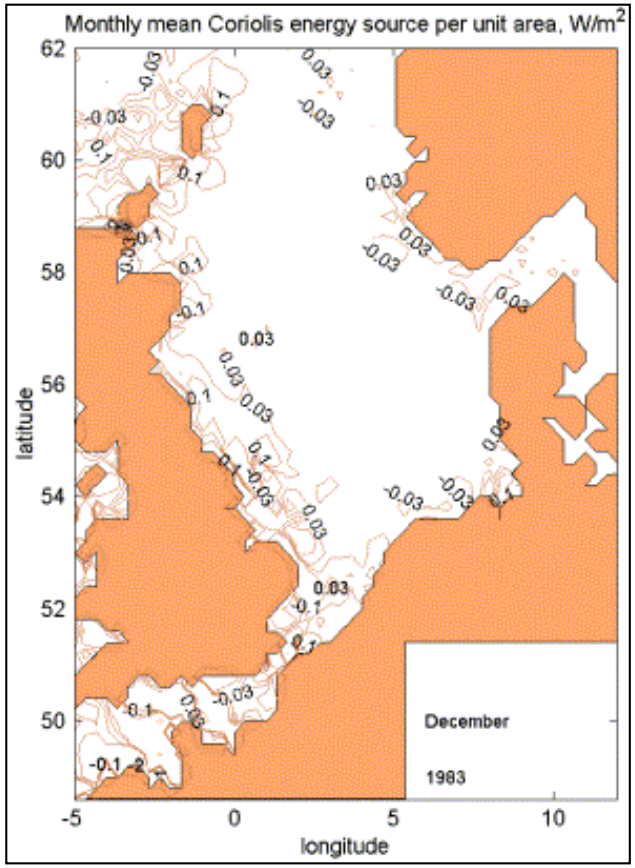

Fig. 6. Mean Coriolis energy source per unit area. Contours are drawn for –4.0, –3.0, –2.0, –1.0, –0.1, –0.03, 0.03, 0.1, 1.0, and 2.0 W m^{-2}.

The first row of Table 2 gives the physical dissipation as determined by means of Eq. (A.9) for the budget region. The annual mean value is 4.2×10^9 W, and the seasonal mean values differ only slightly. The second row gives the numerical dissipation which stems from the model's artificial damping properties, and is determined by balancing the budget. Its annual mean value is 6.2×10^9 W, approximately 13% of the total dissipation, with relatively large variations from summer

(8%) to winter (19%).

Fig. 7 displays the distribution of mean physical dissipation per unit area for December. The dissipation is proportional to the square of current shear, and is therefore large (maximum value >4.5 W m^{-2}) in regions where we find strong tidal activity and high shears, typically along the British coast. Very little dissipation (<0.01 W m^{-2}) is found along the west coast of Norway.

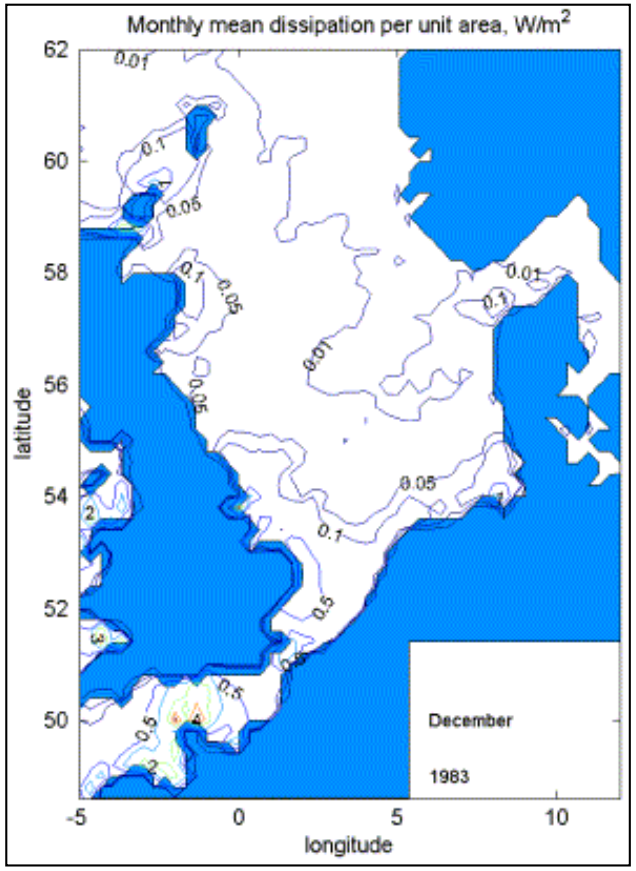

Fig. 7. Mean physical dissipation per unit area for December. Contours are drawn for 0.01, 0.05, 0.1, 0.5, 1.0, 2.0, 3.0, and 4.0 W m^{-2}.

The wind energy input for the same month is shown in Fig. 8. In central parts of the North Sea and along Norway these values are of the same magnitude as the dissipation values (compare Fig. 8 and Fig. 7). But in the areas with strong vertical shear the dissipation values are up to 50 times greater than the wind input values.

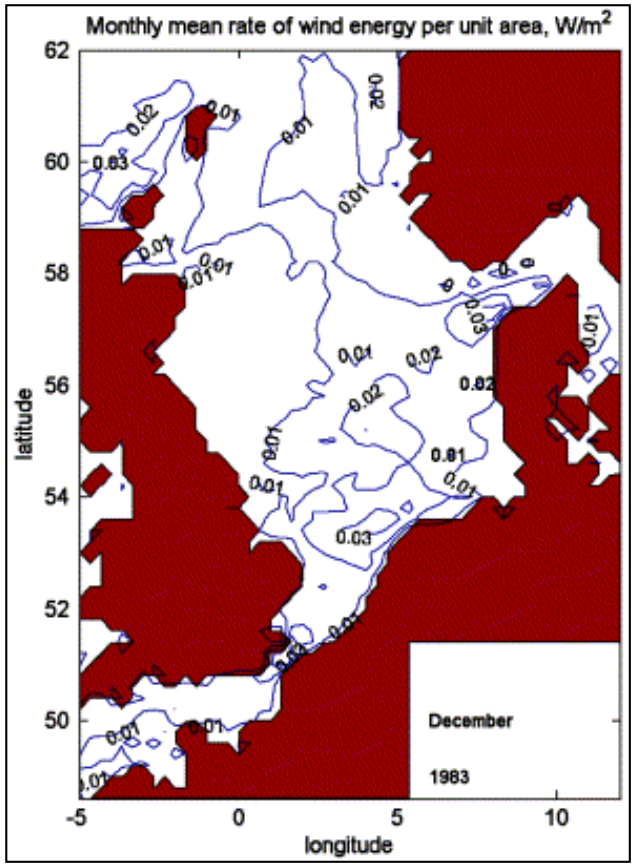

Fig. 8. Mean rate of energy per unit area supplied through winds for December, in W m^{-2}.

The horizontal distribution of the December 1983 monthly mean transport of static energy by the residual and the tidal currents through the three vertical sections are displayed in Fig. 9, Fig. 10 and Fig. 11. The transport values at each grid point represent the flux through the area given by the grid length times the full depth at the grid point. Note that positive values are transport directed out from the North Sea, which means that energy is being transported to the North Sea at points where we find negative values. The lower panel of Fig. 9 reflects the high tidal activity along Scotland contrary to the coast of Norway. Values around 2×10^9 W are found in the western part of the section, while values less than 10% of this are found at the eastern part. The contribution to T from this section is 2.9×10^{10} W, equal to minus the total sum of the values displayed in the lower panel. The contribution of Section 2 to T is a little smaller, equal to 1.8×10^{10} W, but the high tidal activity in the English Channel is reflected in the high local values ranging from 5×10^9 W near England to 2×10^9 W near France, see lower panel in Fig. 10. Skagerrak has low tidal activity, and the contribution to T is only 1.4×10^8 W, all of it found at grid point number 31 in Section 3, see lower panel in Fig. 11.

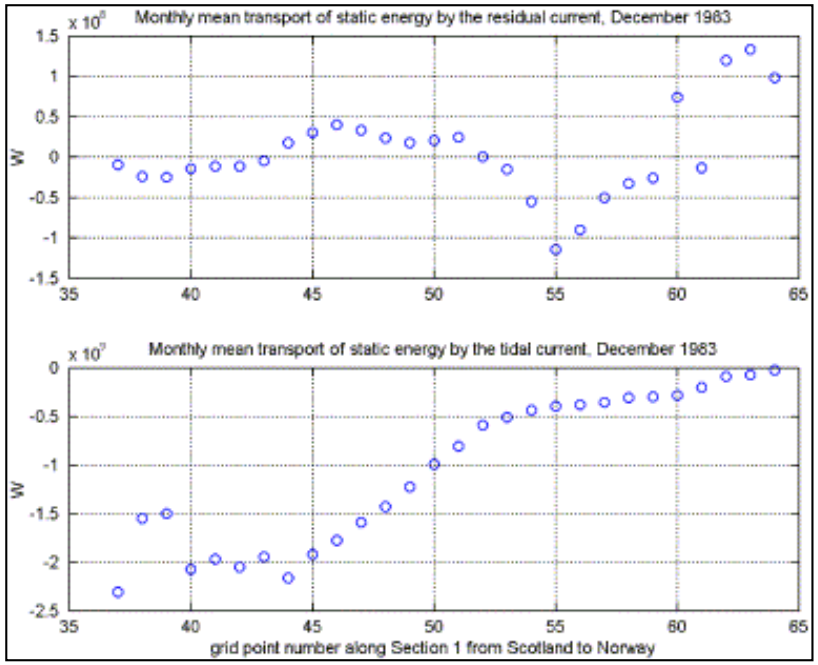

Fig. 9. December 1983 monthly mean transport of static energy through Section 1. The energy flux is integrated over the grid length and the full depth at each grid point along the section. Upper panel: Transport by the residual current, total sum equals 1.3×10^{8} W. Lower panel: Transport by the tidal current, total sum equals -2.9×10^{10} W.

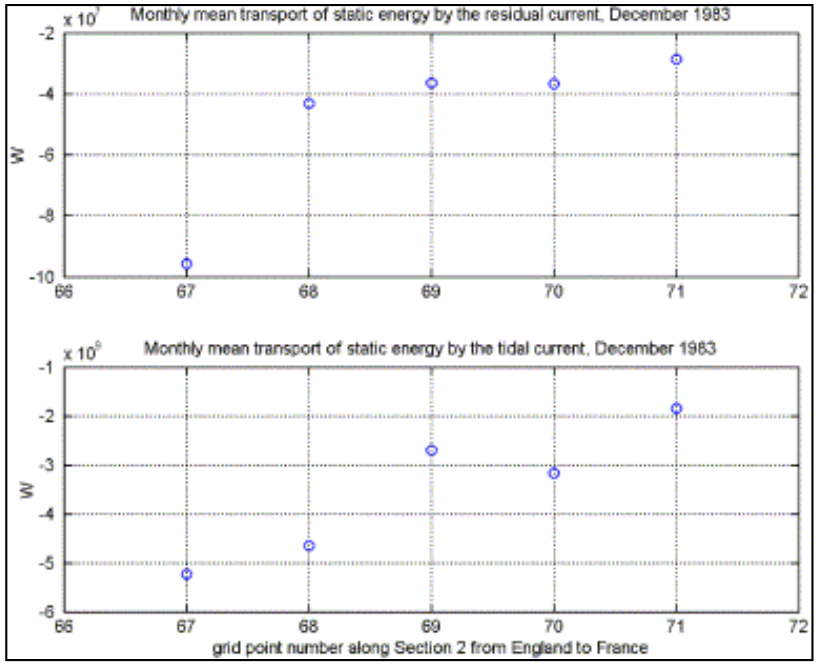

Fig. 10. Same as Fig. 9, but for Section 2. Upper panel: Transport by the residual current, total sum equals -2.4×10^{8} W. Lower panel: Transport by the tidal current, total sum equals -1.8×10^{10} W.

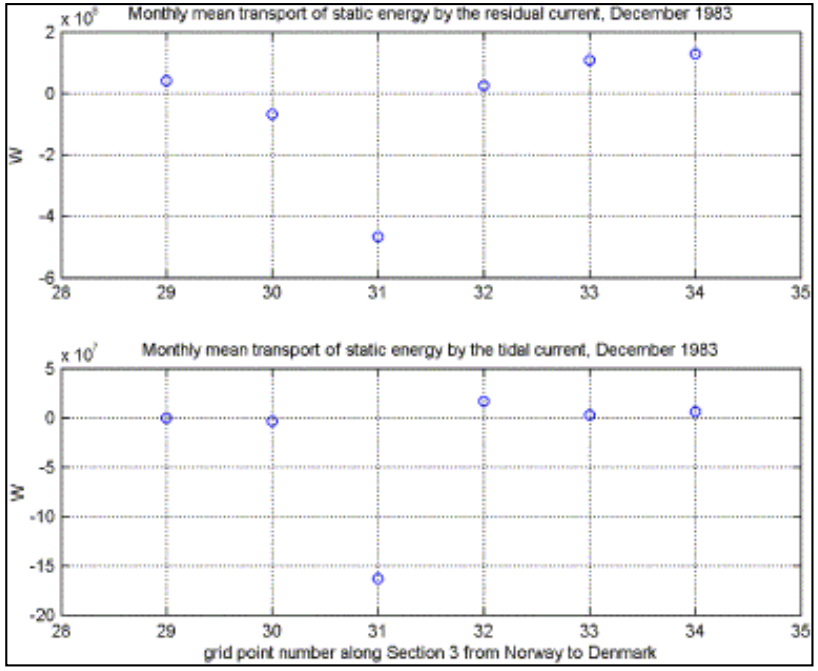

Fig. 11. Same as Fig. 9, but for Section 3. Upper panel: Transport by the residual current, total sum equals -2.4×10^{8} W. Lower panel: Transport by the tidal current, total sum equals -1.4×10^{8} W.

The flux of static energy with the residual current varies temporally (see Fig. 5c), and for December 1983, the monthly mean values are displayed in the upper panels of Fig. 9, Fig. 10 and Fig. 11. Through Section 1, the net static energy flux is directed out of the North Sea and is equal to 1.3×10^{8} W, most of it going with the Norwegian Coastal Current. Strong negative values right outside are connected with the transport of the Dooley Current. Close to Scotland, the flux of static energy by the residual current is small and directed into the North Sea, see Fig. 9 upper panel. The net fluxes through the two other sections are both directed into the North Sea during this month, and happen to be equally large (-2.4×10^{8} W). Again, grid point number 31 in the Skagerrak section gives an extremely large flux value of almost -5×10^{8} W, see Fig. 11 upper panel.

5. Discussion

The energy household of the North Sea, as given by this model experiment, can be inferred by the results in the following way. The net source of energy supply resulting from tidal forcing, wind forcing, and dissipation goes to storage of mechanical energy and export of static and kinetic energy. By examination of Fig. 5, we can see a distinct variation through the year. During summer, there is storage of mechanical energy and net import of static energy, while kinetic energy is exported. For example, in August the import of static energy is large (mainly through the English Channel (Section 2)) and is about 10% of the storage.

During late autumn and winter mechanical energy is lost. During the months of February, March, October, and November mechanical energy is exported, mainly through 1 and 3, while during December and January there is a net import, mainly through 2 and 3. In those two months the numerical dissipation is so high that

there is a net sink of energy in the North Sea of the same size as the artificial Coriolis energy.

Note that the numerical dissipation varies with the wind forcing (compare second row of Table 2 with the tenth row of Table 1), while the physical dissipation is rather constant, and not sensitive to the wind forcing. The model results reveal that bottom friction (first term on the right-hand side of Eq. (A.9)) gives the main contribution (about 90%) to the physical dissipation (not shown). It must be the effect of the tides, since the direct wind forced current is mostly confined to the surface region. Why then do we have this artificial damping, which is seemingly connected to the wind? We can only speculate on the reasons. The nature of numerical dissipation is to damp out the shortest temporal and spatial scales of the current field. Since the wind field is more episodic with stronger bursts in winter than in summer, wind-driven currents will be more episodic during winter than in summer, and will accordingly be subject to stronger numerical damping.

These results show that the kinetic energy storage and transports are much less than those of static energy. The budget region covers a depth range from ten to several hundreds of meters (the Norwegian Trench), which is obviously deep enough to make the static energy storage and transports outrange those of kinetic energy. This disproportionate ratio may also in part be a result of the coarse model resolution. With higher resolution, the currents become narrower and more intense, of which the kinetic energy is higher. This may also explain why the covariance between wind-driven currents and kinetic energy through the three vertical sections is seen to give a seasonal variation of the flux rate of tidal kinetic energy. In the English Channel at cross Section S2 the tidal currents are strong, and the tidal elevations large, so that episodic storm currents should only have a small influence on a 3-month time scale. The model results agree with this assumption for the static energy, where we find a constant flux rate throughout the year at S2 (see row number 15 of Table 1), but not for the kinetic energy (row number 12), because the tidal currents are underestimated. At the Skagerrak Section S3 the tidal signal is weak, so that the effect of covariance between wind-driven currents and energy is seen to give a seasonal variation both for static and kinetic energy flux rate (see row numbers 13 and 16 of Table 1).

The reliability of the results here can be only partly investigated, because few similar works have been done. [Davies and Kwong (2000)] examined the energy fluxes of the tidal components with their shelf model, however excluding meteorological forcing in their model runs. In their Fig. 3a, the M2 tidal energy flux vectors are displayed in W m^{-1}. Thus we may compare the values given in the lower panels of Fig. 9, Fig. 10 and Fig. 11 with Davies and Kwong's vectors along the three Sections S1–S3. If we divide our values by the model's grid length (20 km), we get a flux of 10^5 W m^{-1} in Section 1 close to Scotland, which agrees very well with their results. In the Channel, along Section 2, we get flux values varying from 1×10^5–2.5×10^5 W m^{-1}, which is the same order of magnitude as for the Davies and Kwong numerical runs. In addition, the behaviour along Section 1 compares well with Davies and Kwong's results. However, since Davies and Kwong do not give any integral values for the North Sea, we must rely on former studies.

In Table 3, estimates are listed for energy dissipation in the North Sea calculated by several authors. The value 4.8×10^{10} W found in this work is a little higher than in the former estimates.

Table 3. Estimates of the energy dissipation in the North Sea

Author	Dissipation, 10^{10} (W)
Jeffreys (1920)	4.5
Heiskanen (1921)	4.5
Miller (1966)	4.5
Flather (1976)	4.3
This work	4.8

Some of this difference may be due to the definition of the North Sea budget region. None of the earlier works included any part of the Channel as this work does. Dissipation values in the Channel region are far larger in magnitude than the average for the remaining budget region. (The somewhat odd choice of the location of Section 2 was influenced by the fact that an observation section is located there, and it was useful to compare modelled transports with observed ones.)

6. Conclusion

A mechanical energy budget for the North Sea is calculated based on the results of a three-dimensional baroclinic shelf ocean circulation model. The model was driven by atmospheric data from the year 1983. An annual mean dissipation of 4.8×10^{10} W is calculated for the North Sea, a value close to that found by earlier calculations. The tidal energy input is the largest component of the budget, one order of magnitude greater than the rate of wind energy. Tidal energy input was compared to recent model results and is in agreement with these. Large dissipation occurs where the current shears are large, mainly along the British coast and in the German Bight.

Variations through the year are mainly due to atmospheric forcing. Potential energy builds up during summer, and decreases through winter. For kinetic energy the variation is less pronounced. During winter the transport of mechanical energy is directed out of the North Sea, mainly through the Norwegian Coastal Current, in contrast during summer mechanical energy is imported, mainly through the English Channel. The transport of static energy dominates that of kinetic energy, both that related to the residual and that related to tidal currents.

Acknowledgements

This work has received support from The Research Council of Norway (Programme for Supercomputing) through a grant of computing time.

References

Backhaus (1985). J.O. Backhaus, A three-dimensional model for the simulation of shelf sea dynamics. *German Journal of Hydrography* **38** (1985), pp. 165–187.

Backhaus and Hainbucher (1987). J.O. Backhaus and D. Hainbucher, A finite difference general circulation model for shelf seas and its application to low frequency variability on the North European shelf. In: J.C.J. Nihoul and B.M. Jamart, Editors, *Three-Dimensional Models of Marine and Estuarine Dynamics*, Elsevier, Amsterdam (1987), pp. 221–244.

Baringer and Price (1997). M.O. Baringer and J.F. Price, Momentum and energy balance of the Mediterranean outflow. *Journal of Physical Oceanography* **27** (1997), pp. 678–1692.

Damm (1989). Damm, P., 1989. Klimatologischer Atlas des Salzgehaltes, der Temperature und der Dichte in der Nordsee 1968–1985. Institut für Meereskunde der Universität Hamburg, Technical Report, 6–89, pp. 1–81.

Davies and Kwong (2000). A.M. Davies and S.C. Kwong, Tidal energy fluxes and dissipation on the European continental shelf. *Journal of Geophysical Research* **105** C9 (2000), pp. 21969–21989.

Davies et al (2001). A.M. Davies, P. Hall, M.J. Howarth, P.J. Knight and R.J. Player, Comparison of

observed (HF radar and ADCP measurements) and computed tides in the North Channel of the Irish Sea. *Journal of Physical Oceanography* **31** (2001), pp. 1764–1785.

Erasmi et al (1998). W. Erasmi, G. Siedler and R. Onken, Energy conversion in the Cape Verde Frontal Zone. *Journal of Geophysical Research* **103** C10 (1998), pp. 21469–21479.

Espelid et al (2000). T.O. Espelid, J. Berntsen and K. Barthel, Conservation of energy for schemes applied to the propagation of shallow-water inertia-gravity waves in regions with varying depth. *International Journal for Numerical Methods in Engineering* **49** (2000), pp. 1521–1545.

Flather (1976). R.A. Flather, A tidal model of the North-west European continental shelf. *Mémoires Société Royale des Sciences de Liége* **6** (1976), pp. 141–164.

Goddard and Philander (2000). L. Goddard and S.G. Philander, The energetics of El Niño and La Niña. *Journal of Climate* **13** (2000), pp. 1496–1516.

Hainbucher et al (1987). D. Hainbucher, T. Pohlmann and J.O. Backhaus, Transport of conservative passive tracers in the North Sea: first results of a circulation and transport model. *Continental Shelf Research* **7** (1987), pp. 1161–1179.

Heiskanen (1921). W. Heiskanen, Über den Einfluss der Gezeiten auf die säkuläre Acceleration des Mondes. *Annales Academiae Scientiarum Fennicae* **18** (1921), pp. 1–84.

Jeffreys (1920). H. Jeffreys, Tidal friction in shallow seas. *Philosophical Transactions of the Royal Society of London* **221** (1920), pp. 239–264.

Jeffreys (1952). H. Jeffreys, Tidal friction. In: H. Jeffreys, Editor, *The Earth; Its Origin, History and Physical Constitution*, Cambridge University Press, Cambridge (1952), pp. 217–248.

Kunze et al (1995). E. Kunze, R.W. Schmitt and J.M. Toole, The energy balance in a warm-core ring's near-inertial critical layer. *Journal of Physical Oceanography* **25** (1995), pp. 942–957.

Miller (1966). G.R. Miller, The flux of tidal energy out of the deep oceans. *Journal of Geophysical Research* **71** 10 (1966), pp. 2485–2489.

Pohlmann (1996a). T. Pohlmann, Predicting the thermocline in a circulation model of the North Sea—Part 1: model description, calibration and verification. *Continental Shelf Research* **16** (1996), pp. 131–146.

Pohlmann (1996b). T. Pohlmann, Calculating the annual cycle of the vertical eddy viscosity in the North Sea with a three-dimensional baroclinic circulation model. *Continental Shelf Research* **16** (1996), pp. 147–161.

Pohlmann (1996c). T. Pohlmann, Calculating the development of the thermal vertical stratification in the North Sea with a three-dimensional baroclinic circulation model. *Continental Shelf Research* **16** (1996), pp. 163–194.

Pohlmann (1996d). T. Pohlmann, Simulating the heat storage in the North Sea with a three-dimensional circulation model. *Continental Shelf Research* **16** (1996), pp. 195–213.

Provost and Lyard (1997). C.L. Provost and F. Lyard, Energetics of the M_2 barotropic ocean tides; an estimate of bottom friction dissipation from a hydrodynamic model. *Progress in Oceanography* **40** (1997), pp. 37–52.

Røed and Shi (1999). L.P. Røed and X.B. Shi, A numerical study of the dynamics and energetics of cool filaments, jets and eddies off the Iberian Peninsula. *Journal of Geophysical Research* **104** C12 (1999), pp. 29817–29841.

Appendix A

The mean rate of change of the kinetic and potential energy over a period $t=t_f-t_i$ is given by

$$\frac{1}{t}\int_{t_i}^{t_f}\frac{\mathrm{d}(K+P)}{\mathrm{d}t}\,\mathrm{d}t = \frac{1}{t}(K(t_f)+P(t_f)-K(t_i)-P(t_i)). \tag{A.1}$$

i.e. by taking the difference between evaluations of (2.1) and (2.2) at the end t_f and the start t_i of the period.

We neglect the small transport of kinetic energy through the sea surface. Thus the time mean net transport of kinetic energy through the open boundaries is comprised of contributions from the three vertical sections

$$\frac{1}{t}\int\int\int\rho\,\frac{u^2+v^2}{2}\,\bar{v}\cdot\bar{n}\,\mathrm{d}S\,\mathrm{d}t = \frac{1}{t}\int\sum_{i=1}^{3}\int\int\rho_i\,\frac{u_i^2+v_i^2}{2}\,\bar{v}_i\cdot\bar{n}\,\mathrm{d}S_i\,\mathrm{d}t. \tag{A.2}$$

Similarly for the mean transport of static energy through the open boundaries, however, here the free surface cannot be neglected

$$\frac{1}{t}\int\int\int(\rho g z + p)\bar{v}\cdot\bar{n}\,\mathrm{d}S\,\mathrm{d}t = \frac{1}{t}\int\left[\int\int_A \rho_0 g\zeta w_0\,\mathrm{d}x\,\mathrm{d}y + \sum_{i=1}^{3}\int\int(\rho_i g z + p_i)\bar{v}_i\cdot\bar{n}\,\mathrm{d}S_i\right]\mathrm{d}t. \quad \text{(A.3)}$$

Here w_0 is the net evaporation rate, and ρ_0 is the density of fresh water.

Finally, the mean rate of energy dissipation, Γ, and energy supplied through winds, W, can be evaluated from the stress term in the momentum equation multiplied by the current vector and integrated in space and time. By means of partial derivation this gives

$$\frac{1}{t}\int\int\int_A\int_{-H}^{\zeta}\bar{v}\cdot\frac{\partial\bar{\tau}}{\partial z}\,\mathrm{d}z\,\mathrm{d}x\,\mathrm{d}y\,\mathrm{d}t = \frac{1}{t}\int\left[\int\int\int_A\int_{-H}^{\zeta}\frac{\partial}{\partial z}(\bar{v}\cdot\bar{\tau})\,\mathrm{d}z\,\mathrm{d}x\,\mathrm{d}y - \int\int\int_A\int_{-H}^{\zeta}\bar{\tau}\cdot\frac{\partial\bar{v}}{\partial z}\,\mathrm{d}z\,\mathrm{d}x\,\mathrm{d}y\right]\mathrm{d}t. \quad \text{(A.4)}$$

Here we have neglected the effect of lateral stresses. The first term of the right-hand side is equal to the sum of the work done by surface forces, i.e. both wind stress and bottom friction

$$\frac{1}{t}\int\int\int_A\int_{-H}^{\zeta}\frac{\partial}{\partial z}(\bar{v}\cdot\bar{\tau})\,\mathrm{d}z\,\mathrm{d}x\,\mathrm{d}y\,\mathrm{d}t = \frac{1}{t}\int\int\int_A\left(\bar{v}_\zeta\cdot\bar{\tau}_W\right)\mathrm{d}x\,\mathrm{d}y\,\mathrm{d}t - \frac{1}{t}\int\int\int_A(\bar{v}_{-H}\cdot\bar{\tau}_{-H})\,\mathrm{d}x\,\mathrm{d}y\,\mathrm{d}t \quad \text{(A.5)}$$

with

$$W = \frac{1}{t}\int\int\int_A(\bar{v}_\zeta\cdot\bar{\tau}_W)\,\mathrm{d}x\,\mathrm{d}y\,\mathrm{d}t. \quad \text{(A.6)}$$

Here $\bar{\tau}_W$ is the wind stress. The second term of the right-hand side of Eq. (A.4) is the deformation work which in our case of an incompressible fluid is equal to the production of turbulent energy, which in turn is nearly equal to the viscous dissipation. The work done against gravity by the turbulence is assumed to be so small in the North Sea that it can be neglected. Let A_v denote the vertical eddy viscosity, then the

shear stress is given by

$$\bar{\tau} = \rho A_v\frac{\partial\bar{v}}{\partial z}. \quad \text{(A.7)}$$

At the bottom a quadratic slip condition is applied

$$\bar{\boldsymbol{\tau}}_{-H} = \rho r \bar{v}_{-H} \sqrt{u^2_{-H} + v^2_{-H}}, \tag{A.8}$$

where r is the coefficient of bottom friction.

Thus the mean rate of energy dissipation can be evaluated by the expression

$$\Gamma = \frac{1}{t} \int\int_A \int \left[(\bar{v}_{-H} \cdot \bar{\boldsymbol{\tau}}_{-H}) + \int_{-H}^{\zeta} \bar{\boldsymbol{\tau}} \cdot \frac{\partial \bar{v}}{\partial z} \, dz \right] dx \, dy \, dt. \tag{A.9}$$